PHYSICAL REVIEW B VOLUME 24, NUMBER 2 15 JULY 1981

Local fields at the surface of noble-metal microspheres

Barbara J. Messinger, K. Ulrich von Raben, Richard K. Chang, and Peter W. Barber*

Department of Engineering and Applied Science, Yale University, New Haven, Connecticut 06520

(Received 8 December 1980; revised manuscript received 2 February 1981)

Enhancement of the Raman scattering and fluorescence emission on noble metals (Ag, Cu, and Au) is believed to be caused in part by large local fields at the incident wavelength on the surface of metallic microstructures, such as colloidal suspensions and surface roughness on electrodes and thin films. For metallic spheres immersed in water, calculations are made of the integrated near-field intensity efficiency (Q_{NF}) and that part associated only with the radial field component as a function of incident wavelength (200 – 1200 nm) and sphere radius (0 – 300 nm) which exceeds the usual Rayleigh limit and extends well into the Lorenz-Mie region. The calculated wavelength and radius dependencies of Q_{NF} are compared with those for the better-known efficiencies: extinction (Q_E), far-field scattering (Q_{sca}), and absorption (Q_{abs}). The peak values of these efficiencies have been evaluated when the incident wavelength is in resonance with dipolar and multipolar surface-plasmon modes of Ag, Cu, and Au spheres of varying radii immersed in water.

INTRODUCTION

Giant enhancement ($10^5 - 10^6 \times$) of the inelastic optical scattering efficiency from Raman-active[1–4] and fluorescent molecules[5,6] situated on or near the surface of noble metals (Ag, Cu, and Au) has recently received considerable attention. Although controversy exists among theorists as to the physical mechanisms giving rise to surface-enhanced Raman scattering (SERS) and enhanced fluorescence, most experimental results on SERS for metal electrodes in an electrochemical environment, metal films in vacuum, air, or liquid, and metal colloidal suspensions indicate that some form of local microstructure (sizes between 1 and 100 nm) is necessary. For electrodes or films, the microstructure is provided by surface roughness while, for colloid suspensions, it is provided by the individual particles.

One microstructure model which is receiving a great deal of attention involves microparticle-morphology-defined resonances.[4,7–15] Although the details of this model differ among theorists, one feature is common. At resonance with these microparticle modes, the local electric field at the incident frequency ($\hbar\omega_i$) becomes large near and on the particle surface. Furthermore, the reradiation efficiency of Raman-active or fluorescent molecules situated near and on the surface also becomes enhanced when the inelastically scattered frequency ($\hbar\omega_s$) is also in resonance with these modes. Microparticle models can provide both quantitative results for nonaggregated colloid suspensions and qualitative insight into the role of the surface roughness.

The interaction of electromagnetic waves with metallic microparticles can be treated using the same formalism as for dielectric microparticles.[16,17] Previous dielectric calculations have solved for the extinction (attenuation of the beam in the forward direction) and scattering (far from the microparticle) for spheres, cylinders, and spheroids. Only recently, calculations for the field within a dielectric sphere and cylinder have led to a detailed characterization of the internal absorption by absorbing molecules[18] and inelastic reemission by Raman-active or fluorescent molecules embedded within these dielectric microparticles.[19,20] Sharp resonances which are highly sensitive to the morphology of dielectric spheres and cylinders have been studied theoretically[21,22] and observed experimentally in the optical range for optical levitation[23] and inelastic reemission.[24] These morphology-defined resonances correspond to natural modes of oscillation of dielectric objects. At specific $\hbar\omega_i$ that can excite one of the many resonances, large electric fields within, near, and on the surface of the dielectric microparticle can occur, causing the extinction, elastic scattering (thus optical levitation), and internal absorption to exhibit sharp peaks. Similarly, for specific $\hbar\omega_s$, which can also excite one of these resonances, large Raman or fluorescent emission can be detected regardless of whether the Raman-active or fluorescent molecules are embedded within or coated on the surface of the dielectric microparticle.[25] Experiments[24] have shown that the resonances associated

with the reemission by these molecules at $\hbar\omega_s$ are identical to those which can be probed by tuning the incident wave to equal $\hbar\omega_s$. Even larger inelastic emission can result when both $\hbar\omega_i$ and $\hbar\omega_s$ are in resonance with two different natural modes of oscillation for a particular dielectric microparticle.

Morphology-defined resonances also exist for metallic microparticles and are associated with the surface plasma (SP) resonances of these metal particles. For isolated spheres with radius a, much smaller than the optical wavelength λ (i.e., small-size parameter $ka = 2\pi a/\lambda$), electrostatic calculations can readily solve for the surface-charge density, electric field on and near the metal surface, and the radial dependence of the electric field away from the sphere.[26] The local electric-field intensity in the homogeneous surrounding medium with an index of refraction of n_0 is modified by an amount $[\epsilon(\omega) - n_0^2]^2/[\epsilon(\omega) + 2n_0^2]^2$, where $\epsilon(\omega) = \epsilon_r(\omega) + i\epsilon_i(\omega)$ is the complex dielectric constant of the metal sphere. In this Rayleigh limit, dipolar SP resonance occurs at $\epsilon_r(\omega) = -2n_0^2$ and large enhancement of the local-field intensity can result for metals with $\epsilon_i(\omega) << 1$.[10,11] Because of the partial cancellation in $\epsilon_r(\omega)$ from the *sp*-band electrons [large negative values of $\epsilon_r(\omega)$] and the *d*-band electrons [large positive values of $\epsilon_r(\omega)$], the noble metals such as Ag, Cu, and Au have $\epsilon_r(\omega)$ near $-2n_0^2$ and reasonably small $\epsilon_i(\omega)$ for $\hbar\omega$ in the blue region for Ag and in the green-red region for Cu and Au.[27] These are convenient ranges for existing tunable dye lasers. Unlike the characteristic modes of oscillation for dielectric microparticles, the dipolar SP resonances for metal microparticles are not so sensitively dependent on ka. Thus, for a small metal sphere and small inelastic shifts ($\hbar\omega_s \simeq \hbar\omega_i$), both the radiations at $\hbar\omega_i$ and $\hbar\omega_s$ can be within the dipolar SP resonance linewidth, resulting in an overall enhancement approximately equal to $[\epsilon_r(\omega) - n_0^2]^4/\epsilon_i^4(\omega)$. Within this dipolar SP resonance condition for $\hbar\omega_i$ and $\hbar\omega_s$, the distance dependence for the inelastic intensity from molecules located at position R from the center of the metal sphere ($R \geq a$) is $(a/R)^{12}$, since the electric-field intensity at $\hbar\omega_i$ has an $(a/R)^6$ dependence and at $\hbar\omega_s$ has another $(a/R)^6$ dependence. For metallic microparticles with prolate and oblate spheroidal shapes, similar electromagnetic formalism has been reported.[4,13–15] Calculations have recently been made of the local electric-field enhancement of sinusoidal gratings with noble metal coatings,[28] as well as of metallic spheres and spheroids (with size parameter in the Rayleigh limit) situated near a flat metallic substrate.[13,15]

Beyond the Rayleigh limit, other than dipolar SP resonances can be excited and the effect of phase retardation from different parts of the microparticle must be taken into account. The Lorenz-Mie formalism can be readily applied to metallic spheres with $ka \geq 0.5$, solving for the extinction and far-field elastic scattering. However, while it is quite straightforward to calculate the local electric field on and near metallic spheres of any radius, the theoretical problem of solving the reradiation from Raman-active and fluorescent molecules located at any position outside of a spherical particle of any size is considerably more difficult. The formalism and calculation for the overall enhancement of inelastic emission from molecules located anywhere outside an Ag sphere with radii of 5, 50, and 500 nm have been presented, combining the enhancements of the local electric field at $\hbar\omega_i$, the image dipole, and reradiation efficiency at $\hbar\omega_s$.[12]

In this paper, we will consider only the enhancement of the local electric-field intensity at $\hbar\omega_i$ as a function of single-sphere radius (from 0–300 nm) and incident wavelength (from 200–1200 nm) for Ag, Cu, and Au using the bulk values for $\epsilon(\omega)$ for each noble metal.[27] The size-wavelength dependence of the local electric-field intensity will explain the evolution of the dipolar and higher-order multipolar SP resonances with increasing radii at a fixed incident wavelength or with increasing wavelength at a fixed sphere radius. The reradiation portion of the SERS or fluorescence is not considered in this paper. Furthermore, the interactions of the enhanced local electric-field intensity with the Raman-active or fluorescent molecules, as well as the image forces associated with the molecules and the metal, are not considered. We have therefore restricted our calculations to one portion of the more complex problem of inelastic scattering from molecules located on or near a metallic surface. However, we believe that knowledge of the size-wavelength dependence of the electric-field intensity can be useful in isolating the local-field enhancement mechanism from other enhancement mechanisms.

THEORY

In this section, we define two new near-field quantities which will be useful in comparing the size and wavelength dependencies of the local electric-field intensity near and on the surface of noble-metal spheres. Since these new quantities are related to and will be compared with the usual electromagnetic efficiencies, we will briefly review the

origin and physical interpretation of the scattering, absorption, and extinction efficiencies. Although these efficiency quantities are defined for particles of any shape, the following discussion specifically applies to spherical particles immersed in a homogeneous surrounding.

Given a sphere illuminated by an incident plane wave, the scattering efficiency Q_{sca} is defined as the ratio of the scattered power and the power incident for a given geometrical cross section. Physically, Q_{sca} is a measure of the ability of a sphere to extract power from an incident wave and redirect it as scattered power over all solid angles. For a given set of sphere parameters, Q_{sca} can be considerably greater than unity, which implies that the influence of the sphere on the incident wave extends beyond its geometrical boundaries. Thus, a sphere (metallic or dielectric) can act as a field intensifier, i.e., the strength of the local fields about the sphere can be considerably greater than that of the incident wave which excited the local fields. Similarly, the absorption efficiency Q_{abs} is a measure of the ability of a sphere to absorb power from an incident wave, i.e., it is the ratio of the power absorbed and the power incident for a given geometrical cross section. The extinction efficiency Q_E is the sum of Q_{sca} and Q_{abs}. In terms of the scattering coefficients of a sphere,[16,17]

$$Q_{\text{sca}} = \frac{2}{(ka)^2} \sum_{n=1}^{\infty} (2n+1)(|a_n|^2 + |b_n|^2) \ , \tag{1}$$

$$Q_E = \frac{2}{(ka)^2} \sum_{n=1}^{\infty} (2n+1)[\text{Re}(a_n + b_n)] \ , \tag{2}$$

$$Q_{\text{abs}} = Q_E - Q_{\text{sca}} \ , \tag{3}$$

where a_n and b_n are the scattering coefficients.

In terms of the scattered electric field $\vec{E}_S$, at distance R from the center of the sphere, Q_{sca} for a unit incident field is

$$Q_{\text{sca}} = \lim_{R>>a} \frac{R^2}{\pi a^2} \int_0^{2\pi} \int_0^{\pi} \vec{E}_S \cdot \vec{E}_S^* \sin\theta \, d\theta \, d\phi \ , \tag{4}$$

where R defines a spherical surface over which the integral is evaluated. The definition is restricted to the far-field ($R >> a$) to ensure that only outgoing fields appear under the integral, i.e., that the integral is a measure of the scattered power. In the far field, the electric field decreases as $1/R$ while Q_{sca} is constant and independent of the radius R of the spherical surface over which it is evaluated, i.e., $R^2 |\vec{E}_S|^2$ is constant.

In the near field of the sphere, the incident plane wave is significantly distorted in order to satisfy the boundary conditions at the surface. For example, for a perfect conductor the electric fields must be normal to the surface, i.e., radial. While the far field consists of electric fields (E_θ and E_ϕ), which are perpendicular to the radial direction, the near field contains a radial component (E_R) as well. A quantity similar to Q_{sca} can be introduced, which gives a measure of the electric-field intensity at the surface of the sphere. A particularly convenient form is to use Eq. (4) but, rather than evaluating for $R >> a$, evaluate for $R = a$, i.e., the surface of the sphere. This quantity, called Q_{NF}, where the subscript stands for near field, is given by

$$Q_{\text{NF}} = \frac{R^2}{\pi a^2} \int_0^{2\pi} \int_0^{\pi} \vec{E}_S \cdot \vec{E}_S^* \sin\theta \, d\theta \, d\phi \Big|_{R=a} \ . \tag{5}$$

Q_{NF} is the near-field form of Q_{sca} and, in the limit $R >> a$, Q_{NF} decreases to the asymptotic value Q_{sca}. While Q_{sca} is a convenient quantity with which to compare the ability of spheres to convert an incident electric-field intensity into far-field scattered intensity, Q_{NF} is a useful measure for comparing the ability of spheres to convert an incident electric-field intensity into near-field intensity. In particular Q_{NF} can be evaluated for Ag, Cu, and Au spheres to obtain a measure of relative near-field intensification as a function of sphere size and incident wavelength.

In terms of the scattering coefficients of a sphere,

$$Q_{\text{NF}} = 2 \sum_{n=1}^{\infty} \{ |a_n|^2 [(n+1)|h_{n-1}^{(2)}(ka)|^2 + n|h_{n+1}^{(2)}(ka)|^2] + (2n+1)|b_n|^2 |h_n^{(2)}(ka)|^2 \} \ , \tag{6}$$

where $h_n^{(2)}$ is the Hankel function of the second kind ($e^{i\omega t}$ time dependence assumed). Equation (6) was obtained by reducing the general expression for the scattered field to the near-field case.[26]

That portion of Q_{NF} due to radial fields only is defined as Q_R and is obtained by evaluating Eq. (5) with $\vec{E}_S = E_R$. In terms of the scattering coefficients of a sphere,

$$Q_R = \frac{2}{(ka)^2} \sum_{n=1}^{\infty} (2n+1)(n+1)n |a_n|^2 |h_n^{(2)}(ka)|^2 \ . \tag{7}$$

Q_R is a measure of the ability of a sphere to convert

an incident electric-field intensity into radially directed electric fields at the surface of the sphere.

Q_{NF} can be larger than Q_{sca} because Q_{NF} (the near-field form of Q_{sca} at $R = a$) involves fields which increase faster than R^{-1} as one moves from the far field to the surface of the sphere. Thus, the integrated near-field intensity includes additional field components which appear only in the near-field region. If molecules such as CN^- and pyridine are attached to the sphere with their higher polarizability axis along the radial direction, the combination of preferential molecular attachment and predominance of E_R for the total near field will result in greatly enhanced coupling of the incident wave (at $\hbar\omega_i$) to the molecule. Furthermore, the near-field molecular polarization (at $\hbar\omega_s$) will contain, in addition to the usual R^{-1}-dependent field components, additional near-field components which normally will not contribute to the far-field radiation (i.e., Raman or fluorescence scattering). However, these near-field components at $\hbar\omega_s$ can now be converted to far-field radiation by coupling with the nearby sphere, which acts as an efficient "antenna" at $\hbar\omega_s$. To the first approximation, the overall inelastic scattering can be estimated as a product of $Q_{NF}(\omega_i)Q_{NF}(\omega_s)$, with each Q_{NF} evaluated at $\hbar\omega_i$ and $\hbar\omega_s$. The exact inelastic reradiation efficiency of course does not equal $Q_{NF}(\omega_s)$, since reciprocity will erroneously force the inelastically scattered wave to be a plane wave propagating in an opposite direction to the incident plane wave. The exact solution for the inelastic scattering has been presented,[12] and it would be interesting to compare the degree of error incurred by approximating the molecular reradiation efficiency and image dipole effects with $Q_{NF}(\omega_s)$.

COMPUTATIONAL RESULTS

All the calculations reported here were performed on an HP-1000 computer. Equations (1)–(3) were used for the standard quantities Q_E, Q_{sca}, and Q_{abs}. For the new near-field quantities Q_{NF} and Q_R, Eqs. (6) and (7) were used, which simplified the computer calculations when compared with the usual technique of solving for E_θ, E_ϕ, and E_R at all points on the surface by the standard Lorenz-Mie program and then numerically integrating to solve for Q_{NF} and Q_R. Specific calculations on the radius-wavelength dependencies of Q_E, Q_{sca}, Q_{abs}, Q_{NF}, and Q_R were made for Ag, Cu, and Au spheres, using the bulk values[27] of $\epsilon(\omega)$ regardless of the particle size. The microparticles are assumed to be immersed in water, $n_0 = 1.33$.

Silver

The radius-wavelength dependencies of the far-field quantities Q_E and Q_{sca} for Ag spheres are shown in Figs. 1 and 2, respectively. The largest peak values (designated in Figs. 1 and 2) are obtained for particles with a radius around 20 nm and near the incident wavelength $\lambda = 400$ nm, placing ka in the Rayleigh region. As the radius increases, retardation becomes important (beyond the Rayleigh limit and into the Lorenz-Mie region) and higher-order SP resonances from magnetic dipoles and electric quadrupoles, for example, give rise to additional peaks in Q_E and Q_{sca}. Similar observations can be made for the radius-wavelength dependence of Q_{NF}. The largest value for $Q_{NF} \simeq 1500$ is achieved for $a \simeq 18$ nm, at the dipolar SP resonance of $\lambda = 400$ nm (see Fig. 3). However, as the radius increases, the magnitude of the additional peaks is significantly smaller. At $\lambda = 375$ nm, we have verified that Q_{NF} does approach zero as the radius approaches zero. However, the results shown in Fig. 3 are for $a \geq 1$ nm.

The effect of retardation and multipole contributions can be illustrated by comparing Q_E, Q_{sca}, Q_{abs}, and Q_{NF} for a small sphere ($a = 22$ nm) and for a large sphere ($a = 100$ nm) in Figs. 4 and 5, respectively. In the Rayleigh limit, for spheres with $a = 22$ nm, all four efficiencies peak at that wavelength, which satisfies the dipolar SP resonance condition. The peak value of Q_{NF} is slightly lower than the maximum value for spheres with $a \simeq 18$ nm (shown in Fig. 3). The values for Q_{sca} and Q_{abs}, which sum up to equal Q_E, are nearly the same as those for $a \simeq 18$ nm spheres. However, for spheres in the Lorenz-Mie region ($a = 100$ nm), the wavelength dependencies of Q_E, Q_{sca}, Q_{abs}, and Q_{NF} are considerably more complicated and the ef-

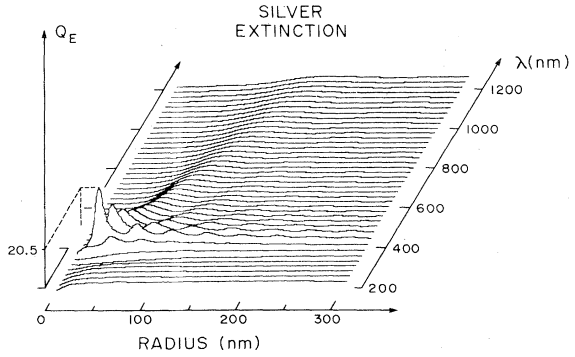

FIG. 1. Extinction efficiency dependence on the incident wavelength and the radius of Ag spheres immersed in water.

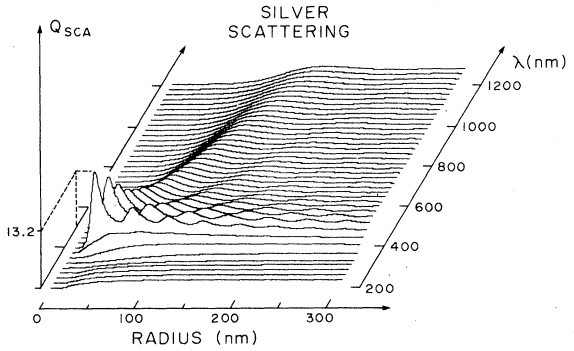

FIG. 2. Far-field scattering efficiency dependence on the incident wavelength and the radius of Ag spheres immersed in water.

ficiencies do not all peak at the same wavelength (see Fig. 5). In fact, the large peak of Q_{NF} is now at $\lambda = 406$ nm and decreases significantly in magnitude compared with that for $a = 22$ nm spheres. Secondary peaks of lower magnitude are present at $\lambda \simeq 500$ and 380 nm, wavelengths which satisfy the higher-order SP resonance conditions. The peaks of Q_{sca} and Q_E are at $\lambda \simeq 480$ nm. Since the amount of absorption by the Ag sphere is a product of $\epsilon_i(\omega)$ and the near- field intensity on the surface to one skin-depth within the sphere, the maximum in Q_{abs} is expected to occur where Q_{NF} is large since $\epsilon_i(\omega)$ is essentially constant in this wavelength region. The extinction (Q_E) for spheres with $a = 100$ nm results mainly from the far-field scattering (Q_{sca}) rather than absorption (Q_{abs}). Since the Raman-active or fluorescent molecules adsorbed on or near the surface of the metal responds to the near-field electric intensity, the correlation in the wavelength dependence of inelastic emission with Q_{NF} will be better than the more readily measured Q_E and Q_{sca}.

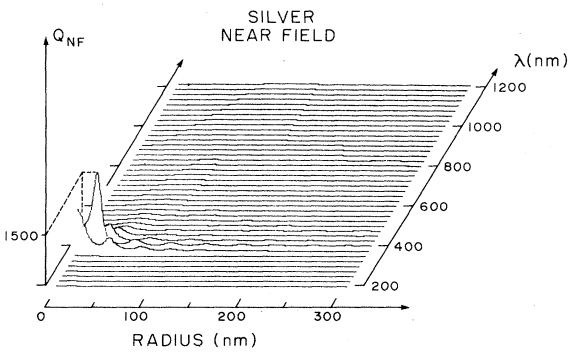

FIG. 3. Dependence on incident wavelength and sphere radius for the near- field scattering efficiency evaluated at the Ag-water interface.

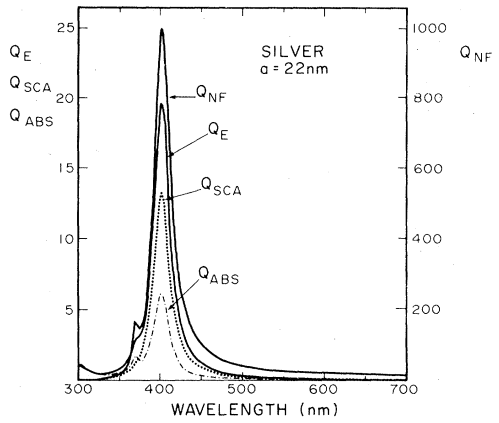

FIG. 4. Extinction, far-field scattering, and absorption efficiency (scale on the left side) compared with the near-field scattering efficiency (scale on the right side) for spheres with $a = 22$ nm immersed in water.

Consequently, any comparison of the wavelength dependence of the Raman or fluorescence intensity with that for Q_E and Q_{sca} should be done with care.

Depending on the orientation of nonspherical molecules adsorbed on the surface of a metal sphere, the radial electric field E_R, which can exist only in the near-field zone of the sphere, can be more effective in polarizing the molecule. Since Q_{NF} consists of the modulus square of E_R , E_θ, and E_ϕ on the sphere surface ($R = a$), we have isolated the radial contribution Q_R from Q_{NF} for spheres with $a = 22$ nm and $a = 100$ nm, respectively. For both size spheres, the Q_R mimics Q_{NF} from $\lambda = 300$ nm to $\lambda = 700$ nm and constitutes more than 70% of Q_{NF} (see Figs. 6 and 7). These results indicate that metallic spheres even with $\epsilon_i(\omega) \neq 0$ convert a large fraction of the plane-wave fields to E_R in the near-field zone of the sphere.

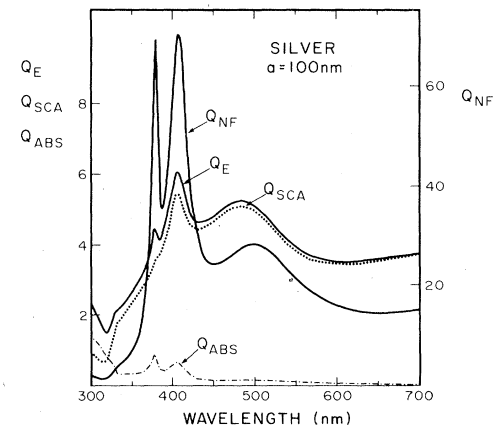

FIG. 5. Same as in Fig. 4, except $a = 100$ nm.

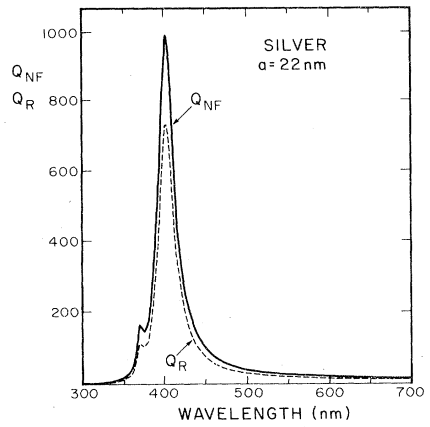

FIG. 6. Comparison of the near-field scattering efficiency with that containing only the radial electric field at the Ag-water interface for spheres with $a = 22$ nm.

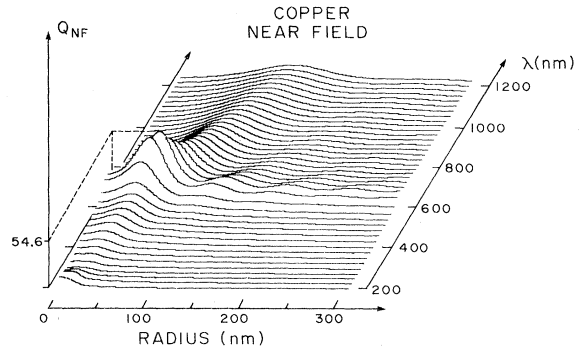

FIG. 8. Dependence on incident wavelength and sphere radius for the near-field scattering efficiency evaluated at the Cu-water interface.

Copper

In many ways, the radius-wavelength dependencies of Q_E, Q_{sca}, and Q_{NF} for Cu are similar to those for Ag. However, for Cu, at the wavelength satisfying the dipolar SP resonance condition, the value for $\epsilon_i(\omega)$ is quite large, resulting in large damping of the dipolar SP mode. The value for $\epsilon_i(\omega)$ is considerably lower at longer wavelengths which can excite higher-order SP modes associated with larger radius spheres. The radius-wavelength dependence for Cu spheres is shown in Fig. 8. The largest peak in Q_{NF} occurs in the Lorenz-Mie region, unlike the case for Ag which has the largest peak occurring in the Rayleigh region.

For Cu spheres with $a = 22$ nm (see Fig. 9), Q_{NF} is peaked at $\lambda \simeq 590$ nm with a magnitude considerably lower than the corresponding value for Ag spheres with $a = 22$ nm. Furthermore, note that $Q_{abs} >> Q_{sca}$ as a consequence of the much larger $\epsilon_i(\omega)$ for Cu compared with that for Ag.

For spheres with $a = 100$ nm (see Fig. 10), the peak of Q_{NF} has broadened and shifted to 950 nm, noticeably displaced in wavelength from the Q_E and Q_{sca} peaks. This result again indicates that it is not necessary to have the peaks of Q_E and Q_{sca} coincide at the same wavelength as the peak of Q_{NF}. The largest value of Q_{NF} for spheres with $a = 22$ nm and $a = 100$ nm is nearly equal, unlike the comparable case for Ag spheres where a large decrease resulted upon going from $a = 22$ nm to $a = 100$ nm. For Cu spheres with $a = 100$ nm, the particles are now sufficiently large causing $Q_{sca} > Q_{abs}$ in spite of the large $\epsilon_i(\omega)$. Since the interband electronic transition sets in around $\lambda \simeq 600$ nm, making $\epsilon_i(\omega)$ even larger, Q_{abs} increases for $\lambda \leq 600$ nm and is significantly displaced in wavelengths from the Q_{sca} and Q_{NF} peaks. The contribution of the radial field Q_R (not shown) is again a sizable frac-

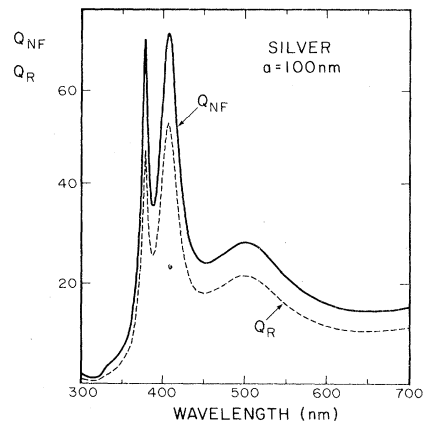

FIG. 7. Same as Fig. 6, except $a = 100$ nm.

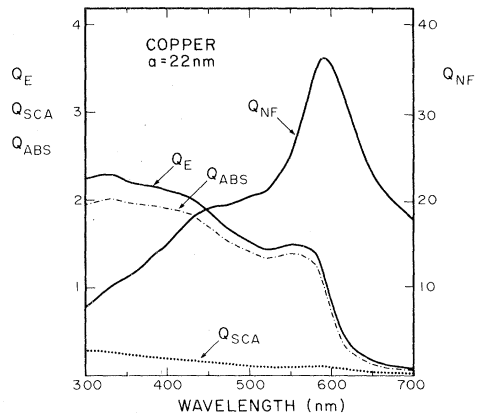

FIG. 9. Same as in Fig. 4, except for Cu spheres with $a = 22$ nm.

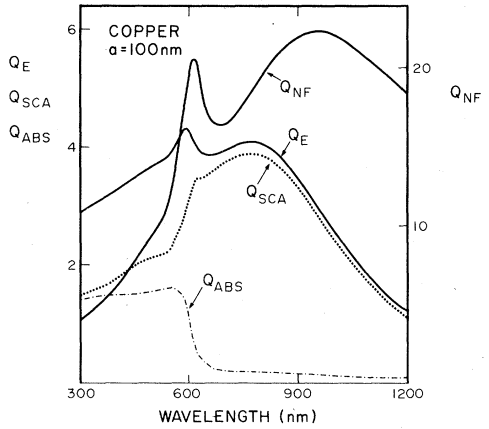

FIG. 10. Same as in Fig. 4, except for Cu spheres with $a = 100$ nm.

tion of Q_{NR} for $a = 22$ nm and $a = 100$ nm Cu spheres.

Gold

Au and Cu spheres have much in common, since both have significantly larger $\epsilon_i(\omega)$ than does Ag at the dipolar SP resonance condition. Again, Q_{NF} has the maximum value for spheres outside the Rayleigh limit where the retardation effect and multipole SP resonances play important roles. The radius-wavelength dependence of Q_{NF} is shown in Fig. 11. The maximum value of Q_{NF} is slightly higher than that for Cu, but significantly lower compared to the maximum value of Q_{NF} in Ag. Even for $a = 22$ nm Au spheres, the peaks of Q_{NF} and Q_E are displaced in wavelength (see Fig. 12). Note that $Q_{abs} >> Q_{sca}$ because of large $\epsilon_i(\omega)$. Again, as a result of the d-level to sp-band electronic transitions, $\epsilon_i(\omega)$ increases for $\lambda \leq 570$ nm, causing Q_{abs} to increase for $\lambda \leq 570$ nm.

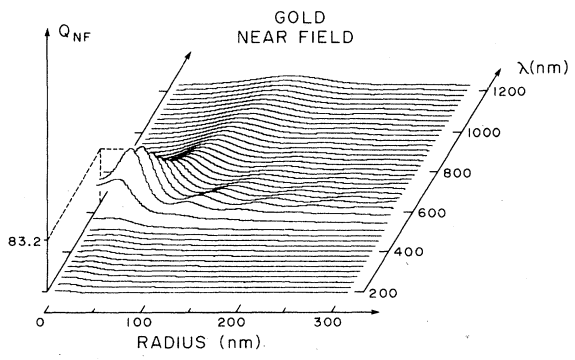

FIG. 11. Dependence on incident wavelength and sphere radius for the near-field scattering efficiency evaluated at the Au-water interface.

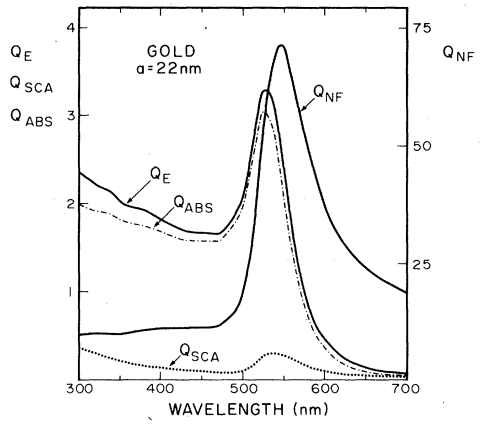

FIG. 12. Same as in Fig. 4, except for Au spheres with $a = 22$ nm.

Upon increasing the radius from 22 to 100 nm, the peak magnitude of Q_{NF} decreases by about $3\times$, and the linewidth for Q_{NF}, Q_E, and Q_{sca} peaks significantly broadens (see Fig. 13). In spite of the large $\epsilon_i(\omega)$, $Q_{sca} > Q_{abs}$. The Q_{sca} peak is displaced from that of Q_{NF} and Q_{abs}. For both $a = 22$ nm and $a = 100$ nm spheres, Q_{abs} peaks at the same wavelength determined by the onset of the increase of $\epsilon_i(\omega)$ when interband electronic transitions occur. Again, the Q_{NF} peak occurs at a longer wavelength than the peaks for Q_E, Q_{sca}, and Q_{abs}.

SUMMARY

Using a new formulation expressed in Eqs. (6) and (7) for the two near-field efficiency quantities, calculations are made of the radius-wavelength dependence of Q_{NF} and Q_R for Ag, Cu, and Au spheres embedded in a homogeneous medium. Be-

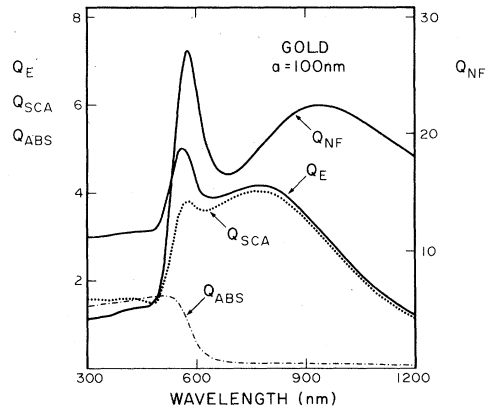

FIG. 13. Same as in Fig. 4, except for Au spheres with $a = 100$ nm.

cause of the $\epsilon(\omega)$ characteristics for these noble metals, dipolar and multipolar SP resonances can be excited, giving rise to significant enhancement in the integrated near-field intensity represented by Q_{NF} and Q_R, as well as far-field efficiency quantities such as Q_E and Q_{sca}. Results indicate that for spheres beyond the Rayleigh limit, retardation and multipole SP resonances give rise to additional peaks in all the efficiency quantities and pull the peak associated with dipolar SP resonances to longer wavelengths. Although the wavelength dispersions of Q_{NF} and Q_R are similiar, they differ from those of the far-field efficiencies Q_E and Q_{sca}, two quantities which are frequently used to compare the wavelength dependence of SERS or fluorescence intensities. Our calculations provide insight into the radius-wavelength dependence of the near-field intensities. The reradiation of the Raman-active and fluorescent molecules after having been induced by the calculated near-field intensities has not been considered. Furthermore, interactions of metal with the chemisorbed molecules (i.e., charge transfer) or the physisorbed molecules (i.e., image effects and polarization of the metal) have not been considered. Thus, our calculations provide only a partial picture of the entire inelastic emission from molecules on or near an isolated metal sphere immersed in a homogeneous medium.

Experiments reported thus far on metallic colloidal suspensions[9,29,30] cannot be readily compared with our results for Q_{NR} and Q_R, even if the reradiation portion is calculated exactly.[12] The addition of pyridine to Au colloids causes chainlike aggregation,[9] while the Ag colloids containing adsorbed citrate also contain aggregated clusters.[29] The extension of our Lorenz-Mie results to randomly shaped clusters is not possible because the internal fields within a large sphere with a radius equal to the cluster are very different from the near fields surrounding each of the spheres forming the cluster. The molecules adsorbed on the surface of each of these spheres will therefore experience a radically different intensity than the internal field (which can be zero) of a large metallic sphere approximating a random cluster. Furthermore, the dipolar SP resonance of an isolated sphere can be significantly modified as the spheres of equal radius start to approach each other with a separation distance of less than $4a$. Consequently, our results are not applicable to any types of aggregates.

Whether SERS observed from electrodes, island film, and colloids is completely caused by the local-field enhancement of the incident radiation near the surface of microstructures remains an open question. A recent report on the experimental observation of SERS from molecules adsorbed on millimeter-sized and smooth mercury droplets[31] leaves the entire topic in a rather confused state. The separation of the local-field contribution from other enhancement mechanisms is partially dependent on understanding the radius-wavelength dependence of the near-field intensities as discussed here for noble-metal spheres. Reviews of the existing theories for SERS other than the local-field enhancements mentioned in this paper have recently been published.[3,32]

ACKNOWLEDGMENTS

We thank Professor Marshall B. Long for his useful advice on the details of the departmental HP-1000 computer, especially the 3D plotting features. We also gratefully acknowledge the partial support of the National Science Foundation (Grant No. ESC79-20113), the Army Research Office (Grant No. DAAG29-79-G-0008), and the Gas Research Institute (Basic Research Grant No. 5080-363-0319) for this research.

*Present address: Departments of Bioengineering and Electrical Engineering, University of Utah, Salt Lake City, Utah 84112.

[1]M. Fleischman, P. J. Hendra, and A. J. McQuillen, Chem. Phys. Lett. 26, 163 (1974).

[2]R. P. Van Duyne, in *Chemical and Biochemical Applications of Lasers,* edited by C. B. Moore (Academic New York, 1978), Vol. 4, p. 101.

[3]A. Otto, Proceedings of the Sixth Solid-Vacuum Interface Conference, Delft, The Netherlands, 1980, unpublished.

[4]E. Burstein and C. Y. Chen, in *Proceedings of the Seventh International Conference on Raman Spectroscopy,* edited by W. F. Murphy (North-Holland, New York, 1980), p. 346.

[5]G. Ritchie, C. Y. Chen, and E. Burstein, Bull. Am. Phys. Soc. 25, 259 (1980).

[6]A. M. Glass, P. F. Lias, J. G. Bergman, and D. H. Olson, Opt. Lett. 5, 368 (1980).

[7]M. Moskovits, J. Chem. Phys. 69, 4159 (1978).

[8]R. M. Hexter and M. G. Albrecht, Spectrochim. Acta 35A, 223 (1979).

[9]J. A. Creighton, C. G. Blatchford, and M. G. Albrecht, J. Chem. Soc. Faraday Trans. II 75, 790 (1979).

[10]S. L. McCall, P. M. Platzman, and P. A. Wolff, Phys. Lett. A 77, 381 (1980).
[11]D.-S. Wang, H. Chew, and M. Kerker, Appl. Opt. 19, 2256 (1980).
[12]M. Kerker, D.-S. Wang, and H. Chew, Appl. Opt. 19, 4159 (1980).
[13]J. L. Gersten and A. Nitzan, J. Chem. Phys. 73, 3023 (1980).
[14]C. Y. Chen and E. Burstein, Phys. Rev. Lett. 45, 1287 (1980).
[15]F. J. Adrian, Chem. Phys. Lett. 78, 45 (1981).
[16]H. C. van de Hulst, *Light Scattering by Small Particles* (Wiley, New York, 1957).
[17]M. Kerker, *The Scattering of Light and Other Electromagnetic Radiation* (Academic, New York, 1969).
[18]P. W. Dusel, M. Kerker, and D. D. Cooke, J. Opt. Soc. Am. 69, 66 (1979).
[19]M. Kerker and S. D. Druger, Appl. Opt. 18, 1172 (1979).
[20]H. Chew, D. D. Cooke, and M. Kerker, Appl. Opt. 19, 44 (1980).
[21]P. Chýlek, J. T. Kiehl, and M. K. W. Ko, Phys. Rev. A 18, 2229 (1978).
[22]G. J. Rosasco and H. S. Bennett, J. Opt. Soc. Am. 68, 1242 (1978).
[23]A. Ashkin and J. M. Dziedzic, Phys. Rev. Lett. 38, 1351 (1977).
[24]R. E. Benner, P. W. Barber, J. F. Owen, and R. K. Chang, Phys. Rev. Lett. 44, 475 (1980).
[25]J. F. Owen, P. W. Barber, P. Dorain, and R. K. Chang, in press.
[26]J. Stratton, *Electromagnetic Theory* (McGraw-Hill, New York, 1951), p. 564.
[27]P. B. Johnson and R. W. Christy, Phys. Rev. B 6, 4370 (1972).
[28]S. S. Jha, J. R. Kirtley, and J. C. Tsang, Phys. Rev. B 22, 3973 (1980).
[29]M. Kerker, O. Siiman, L. A. Bumm, and D.-S. Wang, Appl. Opt. 19, 3253 (1980).
[30]K. U. von Raben, R. K. Chang, and B. L. Laube, in press.
[31]R. Naaman, S. J. Buelow, O. Choshnovsky, and D. R. Herschbach, J. Phys. Chem. 84, 2692 (1980).
[32]T. E. Furtak and J. Reyes, Surf. Sci. 93, 351 (1980).